# Journal Pre-proof

Li conductivity in $Li_{1+x}Ti_{2-x}Al_x(PO_4)_3$ (0.3≤ x≤ 0.7) ceramics prepared from sol-gel precursors

R. Jimenez, I. Sobrados, S. Martinez, M. Criado, B. Perea, J. Sanz

PII: S0925-8388(20)32415-4

DOI: https://doi.org/10.1016/j.jallcom.2020.156051

Reference: JALCOM 156051

To appear in: *Journal of Alloys and Compounds*

Received Date: 26 March 2020

Revised Date: 28 May 2020

Accepted Date: 11 June 2020

Please cite this article as: R. Jimenez, I. Sobrados, S. Martinez, M. Criado, B. Perea, J. Sanz, Li conductivity in $Li_{1+x}Ti_{2-x}Al_x(PO_4)_3$ (0.3≤ x≤ 0.7) ceramics prepared from sol-gel precursors, *Journal of Alloys and Compounds* (2020), doi: https://doi.org/10.1016/j.jallcom.2020.156051.

**R. Jimenez:** Writing - original draft,methodoloy, writing - review & editing, formal analysis**. Sobrados:**Methodology, formal analysis,writing - review & editing. **S. Martinez:** Resources, Investigation, formal analysis. **M. Criado:**Resources. **B. Perea:** Investigation, data curation.**J. Sanz:**Conceptualization, formal analysis, supervision, writing - review & editing.

# Li conductivity in $Li_{1+x}Ti_{2-x}Al_x(PO_4)_3$ (0.3≤ x≤ 0.7) ceramics prepared from sol-gel precursors.

R. Jimenez[a]*,I. Sobrados[a],S. Martinez[a], M. Criado[b], B. Perea[c], J. Sanz [a]

[a.] *Instituto de Ciencia de Materiales de Madrid (ICMM), Consejo Superior de Investigaciones Científicas (CSIC), Cantoblanco, 28049 Madrid, Spain.*
[b.] *Instituto de Ciencias de la Construcción Eduardo Torroja, Consejo Superior de Investigaciones Científicas (CSIC), C/. Serrano Galvache, 4 Madrid. 28033, Spain*
[c.] *Instituto de Óptica Daza de Valdés, Consejo Superior de Investigaciones Científicas (CSIC), C/ Serrano, 121, Madrid, Spain.*

**Keywords:**Energy storage materials, sol-gel processes, ionic conduction, nuclear resonances, vacancy formation.

**Abstract:**

$Li_{1+x}Ti_{2-x}Al_x(PO_4)_3$(LTAP) x = 0.3, 0.4, 0.5 and 0.7) compounds, prepared at 800°C by sol-gel, have been studied by X-ray diffraction, Nuclear Magnetic Resonance, Scanning Electron Microscopy and Impedance Spectroscopy. The increment of lithium enhances Li-Li repulsions, favoring the creation of vacancies at the conduction paths intersection (M1 sites), increasing Li mobility along (…M1-M2-M1…) channels in NASICON phases. The partial elimination of segregated $AlPO_4$, $LiAlP_2O_7$ and $LiTiPO_5$ phases increased Ti, Al solubility in NASICON, improving overall conductivity in ceramics prepared at 950°C. The maximum of "bulk" conductivity was produced in x=0.4 sample, as a consequence of the creation of M1 vacancies and allocation of Li in M2 cavities with optimal Li / vacancy distribution. The presence of secondary phases increased grain boundary impedance, shifting maximum of overall conductivity to x = 0.3compound. Obtained results are compared with those reported previously in LTPA samples prepared by the ceramic route.

## 1. Introduction

NASICON-type materials display an increasing interest because their possible application as solid electrolytes in lithium batteries, sensors, and others electrochemical devices[1]. Ceramic electrolytes with improved chemical and mechanical stability are required to replace liquid electrolytes in safer all solid-state batteries (ASSB)[2,3]. Among solid electrolytes, Li–Al–Ge or Li–Al–Ti phosphates with NASICON structure are good candidates, because their Li mobility and chemical stability against air and moisture; however, electrochemical windows displayed by these electrolytes still remains limited with respect Li metal[4]. Ti based phases are preferable since "bulk" conductivity is larger than that of more expensive Ge counterparts[5-7].

The rhombohedral NASICON phases are built up by $M_2(PO_4)_3$ units in which two $MO_6$ octahedra and three $PO_4$ tetrahedra share oxygen atoms. In conduction paths, Li cations can be allocated at M1 and M2 cavities: in M1, lithium is six-fold coordinated at ternary axes, however, in M2, lithium cations can be accommodated at different interstitial sites. $LiM_2(PO_4)_3$ phases, with R= Ge and Ti, display rhombohedral R-3c symmetry at room temperature[8,9]; but those with Sn, Zr and Hf display triclinic C-1 symmetry[10-12]. In rhombohedral and triclinic phases Li ions occupy respectively M1, and inter-mediate M12 sites allocated between M1 and M2 cavities, see figure 1.

The Li conductivity of $LiTi_2(PO_4)_3$ is near $10^{-6}$ $S.cm^{-1}$ (Ea= 0.45 eV); but, the partial substitution of $Ti^{4+}$ by trivalent cations increased it considerably[13,14]. In $Li_{1+x}Ti_{2-x}Al_x(PO_4)_3$ (LTAP) samples, the maximum conductivity, $3.10^{-3}$ $S.cm^{-1}$ (Ea = 0.3 eV) was achieved in $Li_{1.3}Ti_{1.7}Al_{0.3}(PO_4)_3$ composition at room temperature[15]. For x > 0.4, results are not conclusive, achieving different "bulk" conductivity when the preparation route changes[16,17]. At present the Ti,Al solution limit has not been clearly established.In rhombohedral $LiTi_2(PO_4)_3$, neutron diffraction (ND) refinements showed that most lithium is allocated at M1 sites [8,18]; but in $Li_{1+x}Ti_{2-x}Al_x(PO_4)_3$ series, the incorporation of additional lithium forces lithium to occupy M3 sites (at M2 cavities), see figure 1. The substitution of $Ti^{4+}$ by $Al^{3+}$+ $Li^{+}$ reduces unit-cell dimensions of NASICON phases, but increases Li mobility, indicating that open geometry considerations cannot justify conductivity values, and other factors must be invoked to explain lithium conductivity. In particular, the presence of vacancy at M1 sites (intersection of conduction paths) has been proposed to explain high mobility of lithium in $Li_{1+x}Ti_{2-x}Al_x(PO_4)_3$ series[19]. In these compounds, most probable conduction pathways (...M1-M3-M3'-M1...) were deduced by the maximum entropy method[5].

On the other hand, the Ti/Al solution in NASICON phases is conditioned by formation of secondary $AlPO_4$, $LiAlP_2O_7$ and $LiTiPO_5$ phases. The sol-gel technique increases chemical homogeneity in NASICON precursors, producing a decrease on the preparation temperature. This improves cation solubility and reduces the formation of secondary phases[16]. Since the distribution of segregated phases affects Li grain-boundary conductivity[2], the simultaneous optimization of grain interior and grain-boundary conductivities is required.

In this work, $Li_{1+x}Ti_{2-x}Al_x(PO_4)_3$ samples with nominal $0.3 \leq x \leq 0.7$ compositions have been prepared at 800°C by the sol-gel route and sintered at 950°C to form ceramic pellets. Starting powders and ceramics have been characterized with X-ray (XRD) diffraction, solid state NMR spectroscopy and impedance spectroscopy (IS) techniques. A detailed analysis of $^{27}Al$ and $^{31}P$ MAS-NMR spectra will provide information about Al solution and cation distribution in NASICON phases. $^{7}Li$/ $^{6}Li$ MAS-NMR and Impedance Spectroscopy (IS) have been used to analyze Li mobility; for this purpose, grain interior and grain-boundary conductivities have been resolved as a function of frequency. Information deduced will be used to explain the conduction mechanism and determine the maximum conductivity achieved in the solid-solution $Li_{1+x}Ti_{2-x}Al_x(PO_4)_3$. This information will be useful in preparation of optimized self-supported thick-films electrolytes for all solid-state (ASS) batteries.

## 2. Materials and methods

### 2.1 $Li_{1+x}Ti_{2-x}Al_x(PO_4)_3$ preparation

LTAP samples were prepared by a modified sol-gel route[20]. In preparations, $Ti(OC_4H_9)_4$ was first mixed with ethylene glycol and dripped into a citric acid solution (0.2M) under 3 hours of stirring at 120°C. Stoichiometric $LiNO_3$, $NH_4H_2PO_4$ and $Al(NO_3)_3 \cdot 9H_2O$ were then added to the solution. The molar ratio of citric acid to octahedral [$Li^+$+$Al^{3+}$+$Ti^{4+}$] cations was 3:1 and that of citric acid to ethylene glycol, 1:4. An 1M ammonia solution was finally addeduntil pH~6 was reached, maintaining the stirring until all reagents were dissolved. To enhance estherification and polymerization processes, samples were dried at 170°C overnight. Afterwards samples were heated at 500°C for 4h until complete decomposition of nitrates and organic compounds and heated at 800°C for 5h to form NASICON phases. Obtained powders were mild in an aprotic medium, then 6 mm diameter ceramic pellets were prepared by 2 minutes of uniaxial pressing (173 MPa) and six hours of sintering at 950°C.

### 2.2 Characterization techniques

X-ray diffraction (XRD) patterns were recorded at room temperature, using the Cu-$K_\alpha$ radiation in a Bruker D8 Advance diffractometer (40 kV and 30 mA). XRD patterns were recorded in the 10-70° range, with an angular step 0.04° and a counting time/step of 0.5s. Crystalline phases were identified using International Centre for Diffraction Data (ICDD). Cell parameters were deduced using the Cellref program.

$^{27}Al$, $^{6}Li$/$^{7}Li$ and $^{31}P$ MAS-NMR spectra were recorded with an AVANCE-400 Bruker spectrometer (9.4T magnetic field) working at 104.3, 58.8/155.4 and 161.9 MHz respectively. Spectra were recorded, after 2.0 µs irradiation for aluminium and lithium and 4.0 µs irradiation ($\pi/2$ pulses) for phosphorus, with the MAS technique (10 kHz rotation around an axis inclined 54°44' with respect the external magnetic field). The number of scans was in the range 100-800. The position of NMR components was referred to 85% $H_3PO_4$, 1M LiCl and 1M $AlCl_3$ aqueous solutions. The fitting of NMR spectra was performed with the Winfit program (Bruker), that allowed position, linewidth, and intensity of components to be deduced with a nonlinear least-square iterative method. Quadrupolar $C_Q$ and $\eta$ parameters were deduced with trial and error procedures. $^{27}Al$ NMR chemical shift of components were corrected of second order quadrupolar effects. In quantitative determinations, all spinning sidebands of components were considered.

The surface and cross-sectional microstructure of pellets were examined by scanning electron microscopy (SEM). Sol-gel powders and ceramic broken pellets (fresh fracture)were deposited on a metallic support before analysis in a Phenom. G2 pro SEM Eindhoven, Holland working at 5 kV.

Electrical measurements were performed on ceramic pellets with a 4L-configuration in the 125-350 K temperature interval. For that, sintered pellets were polished and both sides metalized by heating Au

deposited paintings at 800°C (2h). Conductivity measurements were performed under vacuum, upon heating and cooling runs (10 K intervals) in a JANIS VPF 750 cryostat. An automatically controlled Agilent Precision LCR E4980-A analyzer was used for low and medium-frequency measurements (20Hz-2MHz). To extend the frequency range, an Agilent E4991-A RF impedance analyzer (1MHz-3GHz) was used at RT. The Zview software was used to analyze impedance data.

## 3 Results

### 3.1 X-ray diffraction

XRD characterization of $Li_{1+x}Ti_{2-x}Al_x(PO_4)_3$ (LTAP) samples, was performed on powder samples crystallized at 800°C and powder ceramic pellets prepared at 950°C, Fig.2a and b. The most intense XRD peaks correspond to rhombohedral (R-3c) NASICON compounds reported by ICDD (JCDPS file 035–0754). In Al richer LTAP samples, XRD peaks shift toward higher 2θ positions, because of smaller unit cells produced by incorporated $Al^{3+}$ (0.535 Å) with respect $Ti^{4+}$ cations (0.605 Å) (Table 1)[15]. The size of estimated crystallites decreased from 155 nm in Al03, to 84 nm in Al04, and finally to 77nm in Al05 and Al07 sol-gel powders prepared at 800°C. The crystallite size increased up to larger than 1.7 µm after 950°C sintering.
The XRD analysis showed the presence of secondary $LiTiPO_5$ (file 04-011-7990) and $AlPO_4$ (file 00-048-0652) phases. The amount of secondary phases remains small, requiring the zoom of diffraction patterns (12.5° ≤2θ≤ 37.5° region) to identify these phases (insets of Figs. 2a and b). The 950°C sintering decreases intensity of secondary phases and improved crystallinity of samples. The amount of $LiTiPO_5$, however, increased slightly during sintering treatments.

### 3.2 NMR Characterization

$^{27}Al$ (I= 5/2) and $^{31}P$ (I= 1/2) MAS-NMR spectra were used to deduce formed phases[22] and $^{7}Li$ (I=3/2) MAS-NMR spectra to investigate lithium mobility.

#### *3.2.1 $^{27}Al$ MAS-NMR*

Central components of $^{27}Al$ MAS-NMR spectra are formed by two main components (Figure 3a). The most intense component (δ~ -15 ppm) has been associated with octahedral Al of NASICON and the small component (δ~ 40 ppm) with tetrahedral Al of $AlPO_4$ phases. A third component, detected near -18 ppm in Al rich samples, has been ascribed to octahedral Al of the poorly crystallized $LiAlP_2O_7$. Spinning sidebands patterns of $^{27}Al$ MAS-NMR components were used to estimate quadrupolar constants (Table SM1). In quantitative analyses, all spinning side-bands of components were considered. Since quadrupolar interactions modify theintensity of central components, Al MAS-NMR components were only considered in a qualitative way. In general, it was observed that secondary phases decreased at 950°C, but part of $AlPO_4$ and $LiAlP_2O_7$ remained in ceramic samples.

#### *3.2.2 $^{31}P$ MAS-NMR*

In $LiTi_2(PO_4)_3$, the narrow line detected at −27.5 ppm corresponds to $P(OTi)_4$ environments. In $Li_{1+x}Ti_{2-x}Al_x(PO_4)_3$ (0.3≤ x≤ 0.7) samples, this line becomes asymmetrically broadened by new components (Figure 3b). Experimental envelopes were decomposed with the DMFIT program, deducing positions, linewidths, and intensities of Lorentzian/Gaussian (L/G) components. In $^{31}P$ MAS-NMR spectra, components detected at ~ -20 and -30 ppm, have been ascribed to pyrophosphate $LiAlP_2O_7$ (line B) and orthophosphate $AlPO_4$ (line A) phases (see previous section). In agreement with XRD results, the amountof secondary phases decreased but that of $LiTiPO_5$ increased slightly during 950°C sintering (line C at -10 ppm) (Fig. 3b). The quantitative analysis of $^{31}P$ MAS-NMR spectra permitted an estimation of phosphorous in different phases (Table 2).

In NASICON phases, five components ascribed to $P(OTi)_4$, $P(OTi)_3(OAl)$, $P(OTi)_2(OAl)_2$, $P(OTi)(OAl)_3$, $P(OAl)_4$ environments, were detected. As a consequence of Al incorporation, the envelope broadens and shifts towards more positive values (Fig. 3b). The deconvolution of the NASICON band was performed using equally spaced components of the same width. From $^{31}P$ MAS-NMR spectra, Al contents of NASICON phases were estimated, with the expression:

$$\frac{Al^{3+}}{Ti^{4+}} = \frac{4I_4+3I_3+2I_2+I_1}{4I_0+3I_1+2I_2+I_3} = \frac{x}{2-x} \qquad (1)$$

where In (n = 0, 1, 2, 3 and 4) stand for intensity of bands associated with (4-n)Ti.(n)Al environments[15]. In order to reproduce the shape of the $P(OTi)_4$ band, two components of different line-widths, associated with the presence or not of Al as second cation neighbour, were used (see Table SM1). From Al/Ti ratios, Al(x) and Ti(2-x) amounts per NASICON structural formula were deduced (x values of Table 3).

The sintering of $Li_{1+x}Ti_{2-x}Al_x(PO_4)_3$ samples at 950°C produced the partial elimination of $AlPO_4$ and $LiAlP_2O_7$ phases, and the increment of Al in NASICON phases, approaching x values to nominal ones (Table 4). The samples sintering also favoured a small increment of $LiTiPO_5$(Fig. 3b).

*3.2.3 $^7$Li/$^6$Li MAS NMR*

Fig. 4 displays $^7$Li MAS-NMR spectra of sol-gel LTAP powders prepared at 800°C and those obtained by crushing ceramic pellets sintered at 950°C. In $^7$Li MAS-NMR spectra (Fig. 4a), quadrupolar patterns were modulated by (SSB) spinning side-bands (sample rotation); but, in $^6$Li MAS-NMR spectra, smaller interactions reduced dipolar and quadrupolar broadenings, decreasing the number of spinning sidebands (Table 4). The deconvolution of $^7$Li MAS NMR spectra, showed the presence of two components, that at~ -0.7 display larger quadrupolar patterns ($C_Q$~ 60 kHz and η~ 0.3) than that at~ -1.0 ppm ($C_Q$~ 24 kHz and η~ 0). The first component was ascribed to Li ions allocated near M12 windows (M3 sites at M2 cavity) and the second one to Li ions allocated at M1 cavities. In quantitative determinations, all spinning sidebands were considered, producing some differences on relative concentrations deduced from $^7$Li and $^6$Li MAS-NMR spectra. Consideringtheresolution achieved in $^6$Li MAS-NMR spectra, the quantification of detected species has been performed in this signal (Table 4, down).

In Al03 sample, the occupation of M1 sites was higher, but in Al richer samples, M1 and M3 occupations become similar (see Li1/Li1+Li3 ratios deduced from $^6$Li MAS-NMR spectra in Table 4). In ceramic samples heated at 950°C, Li is preferentially allocated at M3 sites. The line-width of central components increased in powdered ceramic pellets prepared at 950°C, suggesting that slow exchanges between M1 and M3 sites increased with respect sol-gel powders prepared at 800°C(Fig. 4b).In the sample Al05 heated at 180 °C, the linewidth of components decreases considerably indicating the onset of long-range motions. In agreement with previous works, exchange motions average chemical shifts and quadrupolar parameters of Li species[23]. In Table 4, it is observed that the position of M1 component of the sample heated at 180 °C is shifted towards M3 component, indicating besides the increment of Li at M3 sites, the onset of M1-M3 exchange processes at room temperature.

In Li richer samples, spinning sidebands of $^7$Li MAS NMR spectra, cover more extended regions ($C_Q$> 80 kHz), indicating the existence of a new environment for lithium. In agreement with this observation, XRD and $^{31}$P NMR patterns showed the presence of $LiAlP_2O_7$ and $LiTiPO_5$ phases (third value of columns) (Table 4).

**3.3 Microstructure study**

The micro-structure of 800°C sol-gel powders display particles agglomerates of 1-2 µm sizes in Al03, Al05 and Al07 samples (see Fig 5a, c and d). In Al04 sample, Fig 5b, smaller agglomerates were formed by sub-micron particles. The fracture of ceramic pellets prepared at 950°C was also analyzed. In Al03, Al05, Al04 and Al07 ceramics, bimodal distributions were detected, where 10 µm grains are surrounded by smaller (< 2µm) particles (Fig 5e, g and h), however, Al04 displayed more homogeneous structures (Fig 5f). In all cases, some intra-grain porosity was detected; but in the Al04 sample inter-grain porosity increased considerably (Fig. 5f). It is important to remark that grain sizes deduced by SEM, Fig 5a-d, are much larger than those deduced from powders XRD patterns. This result suggests that big agglomerates are constituted by non-coherent domains.

**3.4 Ion Conductivity**

The Nyquist (Z) plot of the Al04 sample is illustrated in the 20Hz-3GHz frequency range (Fig. 6). The room-temperature impedance response is formed by two poorly resolved semicircles, one at high frequency, and other at mid frequencies. The last semicircle was convoluted with a low frequencies steep increase of the imaginary part of impedance. Based on these observations, three RC circuits were considered in analysis of electric circuits:

1.-Intra-grain or "bulk" contribution (high-frequency semi-circle).

2.-Inter-grain or "grain boundary" contribution (mid-frequency semicircle).

3.-Electrolyte-electrode interface ion-polarization due to the Li blocking at gold electrodes (low frequency spike).

A normalization of impedance data was performed to take account of the electrode area and samples thickness. As Li mobility increases, the characteristic frequency of the "bulk" response increases up to 200 MHz, requiring lower temperature or higher frequency to detect this contribution.

The densification of ceramic pellets was considered to deduce conductivity in NASICON crystallites that form ceramics samples. The volume fraction of NASICON phases was estimated from the relative density and concentration ofphases (Table 6). Deduced NASICON volume fractions were 0.76, 0.64, 0.82 and 0.66 in Al03, Al04, Al05 and Al07 samples. Based on the isotropic crystals model[24], corrections deduced for crystallites conductivity were 1.54, 2.13, 1.35 and 2.04.

In Fig. 7a the broadband (20Hz-3GHz) response of pellets was analyzed at room temperature. From equivalent high- and mid-frequency RC circuits, bulk and overall conductivity values were deduced. The "bulk" conductivity of NASICON phases increased slightly from Al03 to Al05 but decreased considerably in Al07 sample. In the first three cases, one "bulk" response was observed, but in Al07 sample two contributions were detected, (see Table 5). In analyzed samples, overall conductivity decreased with Al; but in Al07 sample, increased with respect Al04 and Al05 samples.In all cases, overall conductivity of ceramic pellets remained below that of commercial OHARA glass-ceramic Li-NASICON films (solid line at $10^{-4}$ S.cm$^{-1}$) (Fig. 7a).

Derivative plots of admittance data are given at RT as a function of frequency in Fig. 7b. In Al03 and Al04 samples, just one minimum related to the "bulk" response was detected;however, Al05 and Al07 samples a second minimum was detected at lower frequencies that was related to compositional heterogeneities.

In general, dc-conductivity adopts the form:

$$\sigma_{dc} = \sigma_0 . \exp(-E/kT) \qquad (2)$$

The Arrhenius plots of "bulk" and "overall" dc-conductivities are given in Fig.8b. The analysis of these plots showed that "bulk" responses are similar; but grain-boundary ones change considerably in samples. Activation energies deduced from "bulk" and “overall" conductivities are given in Table 5. In Al07 sample, two detected bulk-contributions displayed similar activation energy (Table 5).Pre-exponential factors and activated terms of conductivity have been analyzed in Fig. 8a and b, as a function of the Al content of NASICON phases. In Fig. 8a, the dependence of LTAP samples "bulk" conductivity on Al content is depicted. In this plot, blue symbols stand for "crystallite" conductivities obtained from the correction[24] of "bulk" conductivities of NASICON phases, analyzed in this work. A good agreement between "crystallite" ceramic contributions and those reported on single-crystals (red symbols) was achieved[25]. The crystallite conductivity was maximum in Al04, decreasing considerably in Al07 sample.

## *4. Discussion*

### 4.1 Implications in LTAP preparation

In XRD patterns of $Li_{1+x}Ti_{2-x}Al_x(PO_4)_3$ samples, main diffraction peaks correspond to rhombohedral R-3c NASICON phases (JCDPS file 035–0754); however, small peaks of $LiTiPO_5$ (file 044–0083) and $AlPO_4$ (file 00-048-0652) phases were also detected. The $^{31}$P MAS-NMR spectra are formed by different lines ascribed to LTAP and secondary $LiTiPO_5$, $LiAlP_2O_7$ and $AlPO_4$ phases (Fig. 3). Based on these results, the formation of NASICON $Li_{1+x}Ti_{2-x}Al_x(PO_4)_3$ phases was described by the reaction:

$$(1-x)TiP_2O_7 + xLiAlP_2O_7 + LiTiPO_5 \leftrightarrow Li_{1+x}Ti_{2-x}Al_x(PO_4)_3 \quad (3)$$

The $AlPO_4$formation can be described by the reaction:

$LiAlP_2O_7 + LiTiPO_5 \leftarrow\rightarrow AlPO_4 + Li_2O + TiP_2O_7$ (4)

According to expression (4), the detection of $AlPO_4$ and the absence of $TiP_2O_7$ (file 052-1470) bands in $^{31}P$ MAS-NMR spectra, indicates some preference on the incorporation of Ti with respect Al ions in NASICON phases prepared at 800°C.

From $^{31}P$ NMR spectra, the concentration of NASICON phases was estimated to be 99.5, 97.8, 96.9 and 82.5 % in Al03, Al04, Al05 and Al07 pellets sintered at 950°C. In the sample x= 0.7 heated at 950°C, the amounts of $LiTiPO_5$, $LiAlP_2O_7$, $AlPO_4$ and $Li_{1+x}Ti_{2-x}Al_x(PO_4)_3$ were proportional to 1.3: 3.5: 9 and 27.5 (33 total moles). To improve the amount of NASICON phases, displacing the equilibrium in eq. (3) to the right, some excess of $AlPO_4$ (6%wt) and/or $LiTiPO_5$ (8%wt) were added to preparations[26]; but the amount of NASICON phases did not changed appreciably.

**4.2 Al solid solution**

$^{31}P$ and $^{27}Al$ MAS-NMR spectra afford information about phases formed at 800°C and 950°C. However, taken into account that quadrupolar interactions affect intensity of $^{27}Al$ NMR components, the quantification of phases was performed in $^{31}P$ MAS-NMR spectra.

The formation of $LiAlP_2O_7$ and $AlPO_4$ phases reduced the Al content of NASICON phases. Deduced x values increased from 0.3, 0.37, 0.45 and 0.68, deduced in samples prepared at 800°C, to 0.34, 0.41, 0.50 and 0.69 in ceramic Al03, Al04, Al05 and Al07 samples prepared at 950°C (Table 2). In general, the analysis of $^{31}P$ MAS-NMR spectra showed that the samples heating at 950°C increased the Al content of LTAP phases by decreasing the amount of $AlPO_4$ and $LiAlP_2O_7$ phases (Tables 3 and 4). Similar results have been reported recently[15]. In Fig. 9, results obtained in this work are compared with those reported in LTAP ceramic samples of reference 15. Described results differ from those reported here: Al contents achieved in samples directly prepared by the ceramic route are clearly lower and the amount of secondary phases higher[29].

The incorporation of Al in NASICON phases produced the formation of small amounts of the $LiTiPO_5$ phase, suggesting the complete elimination of secondary phases is difficult to achieve, despite that stoichiometry of LTAP phases formed was close to nominal ones.

From the NMR results, information about cation distributions can also be obtained. If Ti and Al are randomly distributed in NASICON phases, intensity of five detected P components should be proportional to $a^4$, $4a^3b$, $6a^2b^2$, $4ab^3$ and $b^4$, where a and b stand for octahedral Ti and Al occupancies. From contiguous NMR components, Al/Ti ratios were deduced with expressions:

$$Al/Ti = I_3/4I_4 = 4I_2/6I_3 = 6I_1/4I_2 = 4I_0/I_1 = b/a \quad (5)$$

Where $I_n$ values stand for intensity of $P(OTi)_{(4-n)}(OAl)_n$ components. Al/Ti values deduced with these expressions differ from those deduced with expression (5) (last column of Table 6), indicating that Ti and Al are not randomly distributed.

The fitting of the $P(OTi)_4$ component required two components of different linewidth, that were associated with the presence or absence of Al as second cation neighbours (see supplementary material Figure SM1). The intensity of $P(OTi)_4$ environment was higher than expected on the random basis, suggesting the formation of Ti rich environments. On the contrary, small intensity of the $P(OAl)_4$ component suggests the existence of some cation ordering, that prevents the presence of 4 Al around the same P tetrahedron. This effect is larger in sol-gel powders than in ceramic samples. In Al05 pellets, Ti/Al ratios are near random, but in Al0.7 sample, they differ considerably. These observations explain limited Ti and Al solutions achieved in LTAP phases and the favourable formation of secondary phases.

**4.3 Li/Al association**

$^{27}Al$ MAS-NMR spectra are formed by three main bands centred at ~40, -15 and -18 ppm that were ascribed to $AlPO_4$, $Li_{1+x}Ti_{2-x}Al_x(PO_4)_3$ and $LiAlP_2O_7$ phases. In the case of LTAP phases, $Ti^{4+}$ is substituted by $Al^{3+}$, and $Li^+$ ions compensate charge deficits created by aluminium. The increment of Li increases Li-Li repulsions favouring the allocation of Li at M3 sites (Li3) and vacancy at M1 sites, what favours Li mobility. However, if $Li^+$ ions are disposed near Al octahedra[27], electrostatic interactions could decrease considerably Li mobility.

The association of Al and Li has been investigated in Al05 sample, where the amount of secondary phases is still moderate (Fig. 10). In this sample, quadrupolar parameters ($C_Q$= 170 kHz, η= 0.7) deduced for octahedral Al (-12/-14 ppm), indicate that the presence of $Li^+$ ions decreases axial symmetry at these sites (Table SM1). Similar results were reported by Emery et al[28], that reported higher quadrupolar constants for NASICON phases. Another component detected at -14/-15 ppm displayed different quadrupolar parameters ($C_Q$= 100kHz, η= 0.7), suggesting that several Al-Li arrangements can be produced in NASICON phases. The amount of Al submitted to strong quadrupolar interactions decreases when mobility of lithium increases at increasing temperatures (Table SM1). A third component, not displaying quadrupolar interactions was detected near -15 ppm. $^{27}$Al MAS-NMR spectra recorded at increasing temperatures showed important changes (Fig. 10). In particular, the $C_Q$ parameter of NASICON components decreased drastically with temperature, confirming the Li/Al association as the main cause for detected anisotropies. In parallel, the amount of Al non submitted to quadrupolar interactions increased considerably with temperature (column 8 of Table SM1). Based on these observations, it was concluded that quadrupolar interactions are relevant in $^{27}$Al MAS-NMR spectra of LTAP samples but are decreased when Li mobility is increased. Thesamples cooling reproduces starting spectra, indicating that Li-Al arrangements are stable at room temperature (Fig. 10).

**4.4 Influence of Li distributionon Li conductivity**

In $LiTi_2(PO_4)_3$, the distance between M1-M1 sites is 6 Å, however, in $Li_xTi_{2-x}Al_x(PO_4)_3$ samples, lithium also occupy M3 sites (Li3) at M2 cavities[19], decreasing Li1-Li3 distances to 3.5 Å,(see figure 1). The increment of Li, enhances electrostatic repulsions, favouring the creation of vacant M1 sites. As previously stated, the allocation of M1 vacancy at conduction channel crossings, improves Li conductivity[15,19].

In NASICON phases, Li1 species are detected at -1.2 ppm and Li3 ones at -0.7 ppm[15]. The intensity of -0.7 ppm increases with the Li content, indicating that M3 sites allocated near M12 windows are preferentially occupied when the amount of Li increases above 1 per structural formula (Table 4). In $^6$Li MAS-NMR spectra of Al05 sample, the presence of two species was confirmed (Fig. 11b).

According to previous works, Li ions placed at M3 sites forces nearest Li1 ions to occupy other adjacent M3 sites. In this model of arrangement, the amount of M1 vacancy increase with x and that of Li3 with 2x. In the sample x= 0, the amount of M3 vacancy will be near 0, but in x= 1, the amount of Li at M1 should decrease strongly. In both cases, the probability for M1-M3 hopping will be low.

In the proposed model, probability for M1-M1 hopping will be given by the expression $C_1.(1-C_3/3).(1-C_1)$, where occupation of M1 and M3 sites are considered[4]. Based on this model, Li conductivity should display a maximum at x~ 0.4 (Fig. 8a). If the amount of Li1 vacancy increases in a rate lower than x, the maximum is shifted to higher Al contents (dotted lines of Fig. 8a), on the contrary if the rate is larger than x the maximum can be displaced to lower values. From $^7$Li/$^6$Li NMR results, the variation of M1 vacancy with x was deduced, explaining the maximum of conductivity detected near x~ 0.4 ($\sigma_{dc}$~ $7.10^{-3}$ S $cm^{-1}$). In this analysis, the discussion of pre-exponential factors confirmed deduced conclusions (black squares of Fig. 8a). The variation of pre-exponential factors with x was similar to that found at RT for individual LTAP crystallite, reported by Redhammer et al.[25,29]. In the case of samples prepared directly by the ceramic route, the maximum was detected near x= 0.3, confirming that vacancy distribution is affected by the preparation method[15].

In a recent study of the $Li_{1+x}Ge_{2-x}Al_x(PO_4)_3$ series, the authors found similar results on the formation of M1 vacancies with the Al content[30]. In this case, the maximum of “bulk” conductivity was located at x = 0.5. Changes on Li1/Li3 and M1 vacancy distribution were deduced from neutron diffraction refinements (Figure 5a, ref. 30). The linear fit of results yielded an increment of M1 vacancy with 0.7x. For this vacancy rate creation model, the maximum was detected at x = 0.5, that agreed with “bulk” conductivity data. In all considered cases, the creation of M1 vacancy in conduction paths increased again linearly with the Li content[14,15].

In the case of x= 0.5 and 0.7 LTAP samples, Li conductivity decreased, detecting two bulk contribution in the conductivity derivative plots, Fig. 7b. This observation has been associated with local changes on the crystallites composition. In the case of x = 0.7, two detected contributions have been ascribed to the formation of core-shell structures[31]. Changes on the Li distribution in NASICON crystallites, could favour the formation of regions with different mobility (two "bulk" contributions). The activation energy obtained for both contributions was however near 0.32 eV, see table 4. Similar results were reported in x > 0.5 samples prepared by the ceramic method[15].

The heating of the Al05 sample produced important changes in $^{7/6}$Li MAS-NMR spectra that illustrate the onset of Li motions in LTAP samples. In particular, central lines become narrower, and outer spinning sidebands decreased, suggesting that Li-network interactions are partially cancelled by Li motion.

In $^{6}$Li MAS-NMR spectra, intensity of M1 sites decreases with temperature, illustrating Li exchanges between M1 and M3 vacant sites (Fig. 11). The sample cooling reproduces starting spectra indicating that starting disposition of lithium is stable. A comparison of $^{27}$Al and $^{6}$Li MAS-NMR results show that Li mobility is responsible for reversible changes detected in two NMR signals.

The analysis of Arrhenius plots indicated that overall conductivity is limited by the grain boundary contribution (Fig 8b). The overall conductivity was maximum in Al03 sample ($\sigma_{overall}$~$2.10^{-5}$ S $cm^{-1}$), indicating that secondary $AlPO_4$, $LiAlP_2O_7$ and $LiTiPO_5$ phases, decrease overall conductivity in Al rich samples. The broad $^{7}$Li MAS-NMR band centred at ~0 ppm confirmed the presence of lithium in $LiAlP_2O_7$ and $LiTiPO_5$ phases.

A decrease of overall conductivity could also be due to micro-cracks produced in ceramic samples by the anisotropic expansion of NASICON particles. The crystallites size is in all cases larger than the critical size required to form micro-cracks in ceramic particles (1.6 μm)[32]. The grain size detected in LTPA ceramics exceeds the critical size, making plausible the micro-cracks formation during heating-cooling processes. The formation of micro-cracks would increase considerably the grain-boundary and overall impedance of the sample. The results described in this work agree with conductivity values reported in x= 0.3 thick films prepared from sol-gel powders ($\sigma_{Overall}$~ $9.10^{-5}$ $S.cm^{-1}$)[33].

## *5. Conclusions*

$Li_{1+x}Ti_{2-x}Al_x(PO_4)_3$ (LTAP) (x= 0.3, 0.4. 0.5 and 0.7) samples, prepared at 800°C by the sol-gel route, have been investigated with XRD, NMR, SEM and IS techniques. In ceramic pellets prepared at 950°C, the amount of secondary $LiAlP_2O_7$ and $AlPO_4$ phases decreased, enhancing the incorporation of Al in LTAP phases. The thermal treatment at 950°C enlarged the cation solubility in LTAP phases to values near to x ~ 0.7.

In frequency conductivity plots, the discrimination of “bulk” and "grain-boundary" contributions was produced. From the "bulk" contribution, that of crystallites was calculated. The substitution of $Ti^{4+}$ by $Al^{3+}$- $Li^{+}$ allowed the incorporation of additional lithium, increasing Li-Li repulsions and improving Li conductivity in NASICON crystallites. The creation of vacancy at M1 sites, in a rate close to Al substitution x, explain the maximum detected in conductivity in the x= 0.4 sample.

Al is not randomly distributed in the NASICON structure, given rise to some clustering. The formation of heterogeneous core-shell structures in Al richer LTAP phases reduces Li conductivity in ceramic samples.

A comparison of conductivity values in samples prepared by different routes, suggest that nature of grain-boundaries and formation of segregated of $AlPO_4$, $LiAlP_2O_7$ and $Li_{0.5}TiO_2$ phases limits Li conductivity of ceramic pellets. The formation of secondary phases explains the shift of the overall conductivity maximum to the Al03 sample. Finally, the micro-cracks formation at grain-boundary could explain reduced overall conductivity and ageing processes during heating-cooling processes.

The elimination of secondary phases and the enlargement of solid solutions are two aspects that must be improved during elaboration of ceramic samples.

## Acknowledgements

This research was funded by Regional and National agencies for financial support: S2013/MIT-2753 project (Comunidad de Madrid), MAT2016-78362-C4-2R and PCIN-2017-110 (M-ERA-net 2016) projects (Education Ministry).We thanks Dr. J. Bartolomé for SEM images recording.

## Credit authorship contribution statement

**R. Jimenez:** Writing - original draft,methodoloy, writing - review & editing, formal analysis**. Sobrados:**Methodology, formal analysis,writing - review & editing. **S. Martinez:** Resources, Investigation, formal analysis. **M. Criado:**Resources. **B. Perea:** Investigation, data curation.**J. Sanz:**Conceptualization, formal analysis, supervision, writing - review & editing.

## References


1 W. Xiaoa, J. Wanga, L. Fana, J. Zhanga, X. Lia. Energy Storage Materials, 2019, 19, 379–400
2 J.W. Fergus. Journal of Power Sources,2010,195, 4554–4569.
3 K.M.Abraham. J. Phys. Chem.Lett. 2015, 6, 830−844.
4 M.Monchak, T. Hupfer, A. Senyshyn, H. Boysen, D. Chernyshov, T. Hansen,K.G. Schell, E.C. Bucharsky, M.J. Hoffmann, H. Ehrenberg. Inorg. Chem., 2010, 55, 2941-2945.
5 P.Hartmann, T.Leichtweiss, M.R.Busche, M.Schneider, M.Reich, J.Sann, P.Adelhelm, J.J.Janek. Phys. Chem. Lett., 2015, 6, 830−844.
6 E.Zhao, F.Ma, Y. Guo and YJin. RSC Advances, 2016, 6(95): 92579-92585.
7 Y.Yoon, J.Kim, C.Park and D. Shin, J. Ceram. Processing Research,2013, 14, 563-566.
8 M. Alami, R. Brochu, J.L. Soubeyroux, P. Graverau, G. le Flem, P. Hagenmuller. J. Solid State Chemistry,1991, 90, 185.
9 D. Tran Qui, S. Hamdoune, J.L. Soubeyroux, E. J. Prince. Solid State Chemistry,1988, 72, 309.
10 E.Morin, J.Angenault, J.C.Couturier, M.Quarton, H.He, J.Klinowski. Eur J Inorg Chem,1997, 34, 947–958
11 M.Catti, S.Stramare, R.Ibberson. Solid State Ionics, 1999, 123,173–180.
12 E.R. Losilla, M.A.G. Aranda, M. Martinez-Lara, S. Bruque. Chem Mater,1997, 9, 678–1685
13 M.A. París, A. Martínez-Juárez, J.M. Rojo, J. Sanz. J. Phys: Condensed Matter, 1996, 8, 5355-5366.
14 H. Aono, N.Imanaka, G.Y.Adachi.Acc., Chem. Res., 1994, 27, 265-270.
15 K.Arbi, S.Mandal, J.M.RojoandJ.Sanz. Chem. Mater, 2002, 14, 1091-1097.
16 S.Breuer, D.Prutsch, Q.Ma, V.Epp, F.Preishuber-Pflugl, F.Tietz, M.Wilkening. J. Mat. Chem., 2015, 3, 21343-21350.
17 V.Epp, Q.Ma,E.M.Hammer, F.Tietz, M.Wikening. Phys. Chem. Chem. Phys., 2015, 17, 32115-32121.
18 A. Aatiq, M. Ménétrier, L. Croguenne, E. Suard, C. Delmas. J. Mater. Chem.,2002, 12, 2971-2978.
19 K. Arbi, M. Hoelzel, A. Kuhn, F. García-Alvarado, J. Sanz. Inorg. Chemistry, 2013, 52, 9290-9296.
20 R.Jimenez, A.del Campo, M.L.Calzada, J.Sanz, S.DKobylianska, B.O.Liniova, AG.Belous,A.V.Ragulya. J. Eur. Ceram. Soc., 2017, 38, 1679–1687.
21 H. Porthault, F. Le Crasa, S. Frangerb. J. Power Sources, 2010, 195, 6262-6267.
22 R.Kahlaoui, K.Arbi, I.Sobrados, R. Jiménez, J.Sanz, R.Ternane.Inorg. Chemistry, 2016, 56, 1216-1224.
23 K.Arbi, M.Tabellout, M.G.Lazarraga, J.M.Rojo,J. Sanz.Phys. Rev. B, 2005, 72, 094302.
24 R. Jiménez. Solid State Ionics, 1996, 90, 233-244.
25 DRettenwander, AWelzl,SPristat, FTietz, STaibl, GJRedhammer, J.Fleig. J. Mater. Chemistry A,2016, 4, 1506-1513.
26 T. Hupfer, E. Bucharsky, K.G. Schell, A. Senyshyn, M. Monchak. M.J. Hoffmann, H. Ehrenberg. Solid State Ionics, 2016, 288, 235-239. T. Hupfer, E. Bucharsky, K.G. Schell, M.J. Hoffmann, Solid State Ionics, 2016,302, 49-53.
27 B.Lang, B.Ziebarth, C.Elsässer. Chem. Mater,2015, 27, 5040-5048.
28 J.Emery, T.Salkus, A.Abramova, M.Barré, A.F.Orliukas. J. Phys. Chem. C, 2016, 120, 26173-26186
29 G.J.Redhammer, D.Rettenwander, S.Pristat, E.Dashjav, C.M.N.Kumar, D.Topa, F.Tietz. Solid State Sciences, 2016,60, 99-107
30 M. Weiss, D.A. Weber, A.Senyshyn,J. Janek, W.G. Zeier. ACS Appl. Mater. Interfaces, 2018, 10, 10935−10944
31 K. Arbi, W. Bucheli, R. Jiménez and J. Sanz. J. Eur. Ceramic Society, 2015, 35, 1477-1484.
32 S.D.Jackman, R.A.Cutler, J. Power Sources, 2012, 218, 65-72.
33 R. Jiménez, I. Sobrados, S. Martínez-Chaparro, A.A. del Campo, M.L. Calzada, J. Sanz, S.Y. Tsai, M.R. Lin, K.Z. Fung, E. Kazakevicius, A Kežionis. Inorganics,2019, 7, 107.

## Figure captions:

Figure 1: Typical crystalline structure of Li- Nasicon compounds.$M^{4+}$/ $M^{3+}$ Octahedron (light blue), $P^{5+}$ tetrahedron (orange). Available Li sites along conduction channels (connected blue lines): M1 (blue), M2 (Violet), M3 (green) and M12 (yellow). M12, M3 and M2 sites are in the so called M2 cavity. M1 site is at the centre of the M1 cavity.

Figure 2: XRD patterns of powder LTAP 03, 04, 05 and 07 samples crystallized at 800°C (a) and powders obtained from ceramics prepared at 950°C (b). Intense peaks correspond to Bragg reflections of NASICON compounds and small ones to secondary $LiTiPO_5$ and $AlPO_4$ phases. In figure a, the zoom at the 22-30 2Θ range in included as insets for the better observation of secondary phases. In figure b, the zoom at the 25-30 2Θ range in included as insets for the better observation of secondary phases.

Figure 3: a) Central $^{27}$Al MAS-NMR components of $Li_{1+x}Ti_{2-x}Al_x(PO_4)_3$ (LTAP) samples. Spectra were recorded on samples prepared by the sol-gel route at 800°C and on powders obtained from pellets sintered at 950°C. b) Central $^{31}$P MAS-NMR components of $Li_{1+x}Ti_{2-x}Al_x(PO_4)_3$ (LTAP) samples. Spectra were recorded on samples prepared by the sol-gel route at 800°C and on powders obtained from pellets sintered at 950°C. Bands centred at -30, -20 and -10 ppm correspond to secondary $AlPO_4$ (A), $LiAlP_2O_7$ (B) and $LiTiPO_5$ (C) phases.

Figure 4: a) $^{7}$Li MAS NMR spectra of $Li_{1+x}Ti_{2-x}Al_x(PO_4)_3$ samples recorded on samples crystallized at 800°C and powders obtained from pellets sintered at 950°C. b) Central components of spectra.

Figure 5: SEM micrographs of a) Al03, b) Al04, c) Al05 and d) Al07 powder samples prepared by sol-gel route at 800°C. e) Al03, f) Al04, g) Al05 and h) Al07 powder samples obtained from fresh fractured ceramics prepared at 950°C.

Figure 6: Impedance Nyquist plot of the Al04 sample at RT.

Figure 7: a) Frequency dependence of conductivity values measured at 300K (20Hz-3GHz) in $Li_{1+x}Ti_{2-x}Al_x(PO_4)_3$, x= 0.3, 0.4, 0.5 and 0.7 ceramic pellets. b) Log conductivity vs log frequency derivative plots of Al03, Al04, Al05 and Al07 samples.

Figure 8: (a) Calculated dependence of $c_1.(1-c_3/_3).(1-c_1)$ probabilities on Al content of NASICON phases. Dash curves were calculated for different distribution models of Li at M1 and M3 sites (see text). Experimental conductivity points are included in the plot as well as results from references 23 and 25. (b) Arrhenius plots of "bulk" and "overall" dc-conductivities of $Li_{1+x}Ti_{2-x}Al_x(PO_4)_3$ (x= 0.3, 0.4, 0.5 and 0.7) samples. In x= 0.7, two "bulk" (Bulk1 and Bulk2) contributions were detected.

Figure 9: Al incorporated in $Li_{1+x}Ti_{2-x}Al_x(PO_4)_3$ phases, as deduced from $^{31}$P MAS-NMR spectra (black squares). In this plot, black squares stand for samples powders from sol-gel treated at 800°C. Red diamonds stand for powders from ceramics sintered at 950°C. Values reported previously in ceramic samples from solid state reaction are included (green triangles) ref. 15.

Figure 10: Temperature dependence of $^{27}$Al MAS-NMR spectra recorded in the x= 0.5 sample. The sample cooling reproduces starting spectra. At increasing temperatures, the amount of Al atoms interacting with Li ions, decreased considerably (see text).

Figure 11: Temperature dependence of $^{6}$Li (b) MAS-NMR spectra of x= 0.5 sample. In these spectra, two lithium species are detected in NASICON phases (see text). The sample heating illustrates exchange motions between Li1 and Li3 species. The samples cooling reproduces starting spectra.

Tabla1: Unit cell parameters of $Li_{1+x}Al_xTi_{2-x}(PO_4)_3$ samples prepared by the sol-gel route.

| x | a (Å) | c (Å) |
|---|---|---|
| **0** | 8.5137[1] | 20.871[1] |
| **0.3** | 8.5051 (15) | 20.841 (24) |
| **0.4** | 8.5024 (18) | 20.837 (29) |
| **0.5** | 8.4985 (17) | 20.812 (26) |
| **0.7** | 8.4862 (57) | 20.869 (101) |

Table 2: Amounts of phosphorous in different phases, deduced from $^{31}P$ MAS-NMR spectra.

| Sample | $AlPO_4$ | $LiAlP_2O_7$ | $LiTiPO_5$ | LTAP |
|---|---|---|---|---|
| **Al0.3 sol-gel** | --- | 0.8 | 0.3 | 98.9 |
| **Al0.3 pellet** | --- | 0.4 | 0.1 | 99.5 |
| **Al0.4 sol-gel** | 7.6 | 4.6 | 1.8 | 86.0 |
| **Al0.4 pellet** | --- | 0.1 | 2.3 | 97.6 |
| **Al0.5 sol-gel** | 7.9 | 7.6 | 0.2 | 84.3 |
| **Al0.5 pellet** | 1.0 | 0.2 | 2.0 | 96.8 |
| **Al0.7 sol-gel** | 12.8 | 7.6 | 1.0 | 78.6 |
| **Al0.7 pellet** | 8.7 | 7.6 | 1.3 | 82.4 |

Table 3: Intensity of $^{31}P$ MAS-NMR components of NASICON phases. From In values of $Ti_{4-n}Al_n$ environments, $x_{Al}$ values were deduced (see text).

| Sample | $I_4$(%) | $I_3$(%) | $I_2$(%) | $I_1$(%) | $I_0$(%) | $X_{nom}$ | $X_{exp}$ |
|---|---|---|---|---|---|---|---|
| **Al0.3 sol-gel** | – | 2.3 | 11.4 | 30.6 | 54.6 | 0.3 | 0.30 |
| **Al0.3 pellet** | – | 0.9 | 11.0 | 43,8 | 43.7 | 0.3 | 0.34 |
| **Al0.4 sol-gel** | – | 2.2 | 13.2 | 31.2 | 39.5 | 0.4 | 0.37 |
| **Al0.4 pellet** | – | 2.7 | 15.1 | 41.7 | 38.1 | 0.4 | 0.41 |
| **Al0.5 sol-gel** | – | 5.2 | 15.3 | 29.7 | 34.0 | 0.5 | 0.45 |
| **Al0.5 pellet** | 0.3 | 4.5 | 20.1 | 41.3 | 30.8 | 0.5 | 0.50 |
| **Al0.7 sol-gel** | 3.8 | 10.6 | 17.9 | 25.7 | 21.1 | 0.7 | 0,68 |
| **Al0.7 pellet** | 2.7 | 11.8 | 18.8 | 30.4 | 18.6 | 0.7 | 0,69 |

Table 4: Positions (δ), widths (w) and percentages (%) of components detected in $^7Li$ and $^6Li$ MAS-NMR of sol-gel and ceramic powders (0.3, 0.4, 0.5 and 0.7 Al samples). Quadrupolar ($C_Q$) constants were deduced from $^7Li$ NMR spectra and $Li1/Li_{tot}$ ratios from $^6Li$ NMR spectra.

| $^7$**Li**/ Sample | Position (ppm) | | | Width (ppm) | | | $C_Q$ (kHz) | | |
|---|---|---|---|---|---|---|---|---|---|
| Al0.3 $_{sol-gel}$ | -1.07 | -0.75 | --- | 0.45 | 2.26 | --- | 30 | 70 | --- |
| Al0.3 $_{pellet}$ | -1.10 | -0.83 | --- | 1.10 | 2.87 | --- | 40 | 80 | --- |
| Al0.4 sol-gel | -1.08 | -0.70 | -0.15 | 0.49 | 1.75 | 1.50 | 30 | 50 | 90 |
| Al0.4 $_{pellet}$ | -0.93 | -0.90 | - | 0.91 | 1.91 | - | 20 | 40 | - |
| Al0.5 $_{sol-gel}$ | -1.01 | -0.65 | -0.05 | 0.55 | 1.30 | 1.50 | 20 | 50 | 100 |
| Al0.5 $_{pellet}$ | -1.15 | -1.00 | - | 0.85 | 2.20 | - | 30 | 54 | - |
| Al05 $_{pellet\ @\ 180ºC}$ | -0.74 | -0.43 | -020 | 0.34 | 0.71 | 2.50 | 15 | 50 | 60 |
| Al0.7 $_{sol-gel}$ | -0.91 | -0.60 | 0.06 | 0.69 | 1.79 | 1.53 | 14 | 70 | 118 |
| Al0.7 $_{pellet}$ | -0.93 | -0.73 | -0.25 | 0.80 | 1.60 | 2.60 | 14 | 110 | 110 |

| $^6$**Li**/ Sample | Position (ppm) | | | Width (ppm) | | | $Li_1$ | $Li_3$ | Lis (%) | $Li_1/Li_1+Li_3$ |
|---|---|---|---|---|---|---|---|---|---|---|
| Al0.3 $_{sol-gel}$ | -1.01 | -0.75 | --- | 0.34 | 1.00 | --- | 68 | 32 | --- | 68% |
| Al0.3 $_{pellet}$ | -1.01 | -0.95 | --- | 0.55 | 1.10 | --- | 68 | 32 | --- | 68% |
| Al0.4 $_{sol-gel}$ | -0.98 | -0.75 | -0.12 | 0.30 | 0.56 | 0.51 | 65 | 31 | 4 | 67% |
| Al0.4 $_{pellet}$ | -0.99 | -0.95 | --- | 0.33 | 0.70 | --- | 51 | 49 | --- | 51% |
| Al0.5 $_{sol-gel}$ | -0.99 | -0.68 | 0.00 | 0.31 | 0.77 | 0.44 | 51 | 31 | 18 | 62% |
| Al0.5 $_{pellet}$ | -1.04 | -1.00 | 0.00 | 0.34 | 0.80 | 0.38 | 53 | 44 | 3 | 54% |
| Al05 $_{pellet\ @\ 180ºC}$ | -0.76 | -0.58 | 0.05 | 0.30 | 0.54 | 0.50 | 43 | 53 | 4 | 45% |
| Al0.7 $_{sol-gel}$ | -0.92 | -0.65 | 0.14 | 0.31 | 1.01 | 0.40 | 22 | 38 | 40 | 37% |
| Al0.7 $_{pellet}$ | -0.88 | -0.73 | 0.05 | 0.40 | 1.00 | 0.51 | 27 | 53 | 19 | 34% |

Table 5: Conductivity corresponding to LTAP ceramic samples.In the Al07 sample two bulk contributions were considered.

| x | $\sigma_{"bulk"}$ ($Scm^{-1}$) @RT | $\sigma_{"crystallite"}$ ($Scm^{-1}$) @RT | $\sigma_{"overall"}$ ($Scm^{-1}$) @RT | $Ea_{"bulk"}$ (eV) | $Ea_{"overall"}$ (eV) |
|---|---|---|---|---|---|
| 0.3 | $3.6\ 10^{-3}$ | $5.6\ 10^{-3}$ | $2.5\ 10^{-5}$ | 0.29 | 0.33 |
| 0.4 | $3.6\ 10^{-3}$ | $7.0\ 10^{-3}$ | $1.4\ 10^{-6}$ | 0.30 | 0.35 |
| 0.5 | $4.5\ 10^{-3}$ | $5.9\ 10^{-3}$ | $4.2\ 10^{-7}$ | 0.30 | 0.46 |
| 0.7 | $7.2\ 10^{-4}/1.5\ 10^{-4}$ | $1.1\ 10^{-3}$ | $1.0\ 10^{-5}$ | 0.32/0.32 | 0.41 |

Table 6: Ti/Al distribution features deduced from relative intensity of $^{31}P$ MAS-NMR components of NASICON phases. Calculated ratios are compared with those deduced from random distributions.

| **Sample Solgel (SG) Pellet (P)** | **x** | **$Ti^{4+}$/ $Al^{3+}$ (2-x/x)** | **$I^3/4I^4$** | **$4I^2/6I^3$** | **$6I^1/4I^2$** | **$4I^0/I^1$** |
|---|---|---|---|---|---|---|
| **Al03- SG** | 0.30 | 5.66 | -- | 3.33 | 3.99 | 7.13 |
| **Al03-P** | 0.34 | 4.88 | -- | 8.22 | 5.92 | 3.99 |
| **Al04- SG** | 0.37 | 4.40 | -- | 4 | 3.54 | 5.06 |
| **Al04 - P** | 0.41 | 3.87 | -- | 3.72 | 4.14 | 3.65 |
| **Al05 - SG** | 0.45 | 3.44 | -- | 1.96 | 2.91 | 4.57 |
| **Al05 -P** | 0.50 | 3.00 | 3.75 | 2.97 | 3.08 | 2.98 |
| **Al07 -SG** | 0.68 | 1.94 | 0.70 | 1.12 | 2.15 | 3.28 |
| **Al07 -P** | 0.69 | 1.89 | 1.09 | 1.06 | 2.42 | 2.45 |

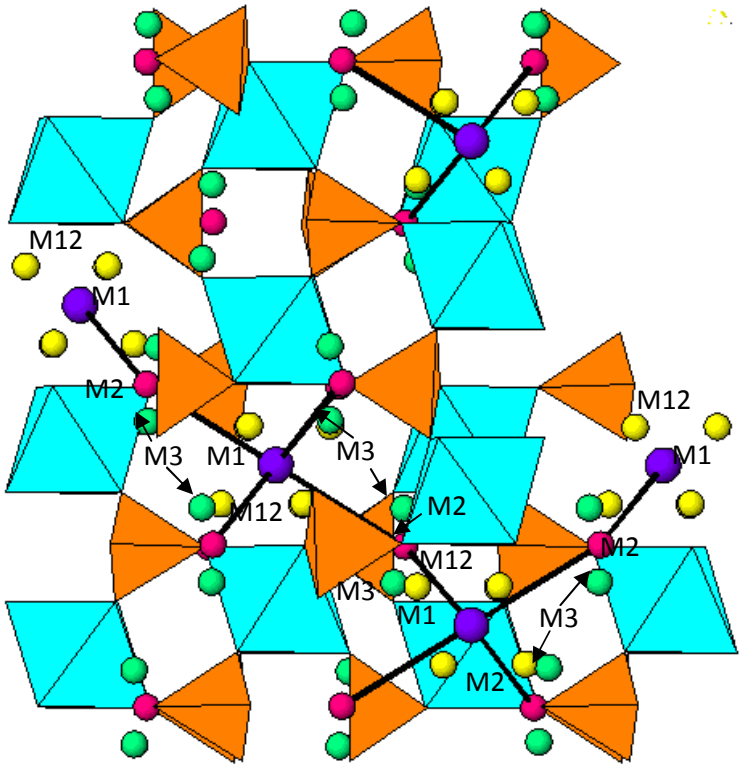


Figure 1.

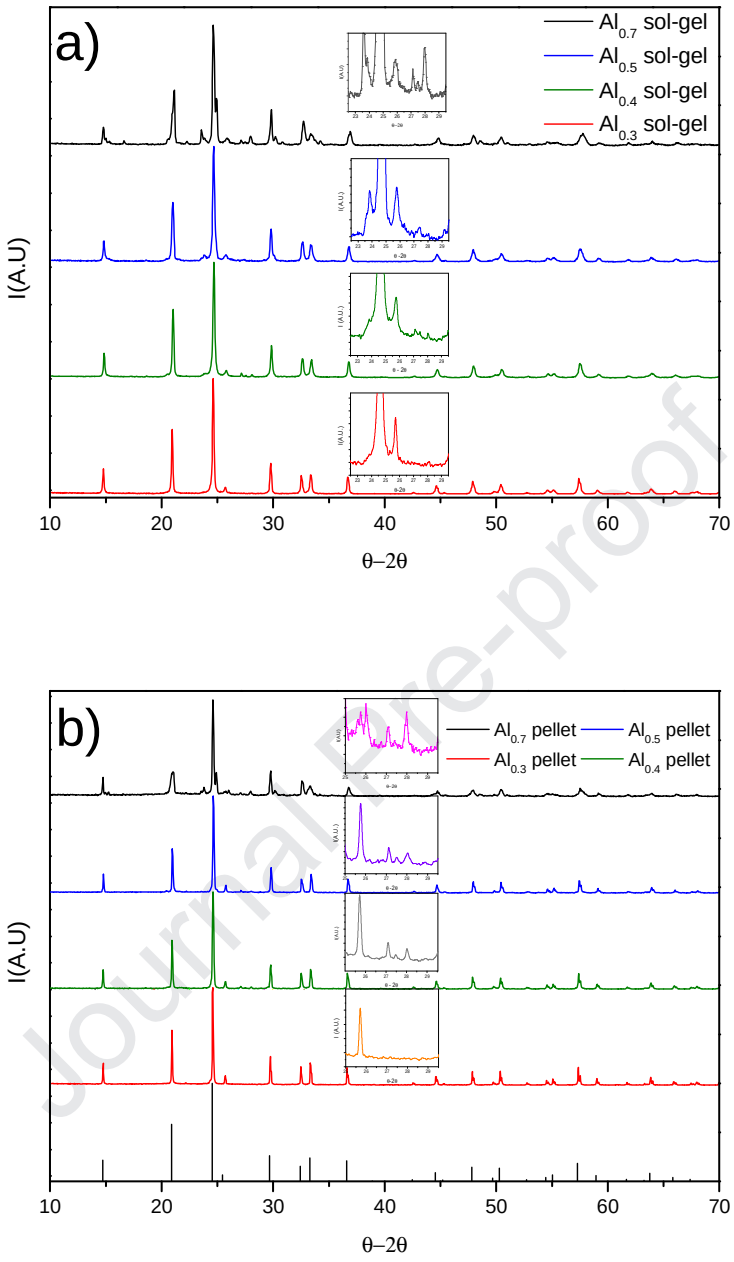


Figure 2.

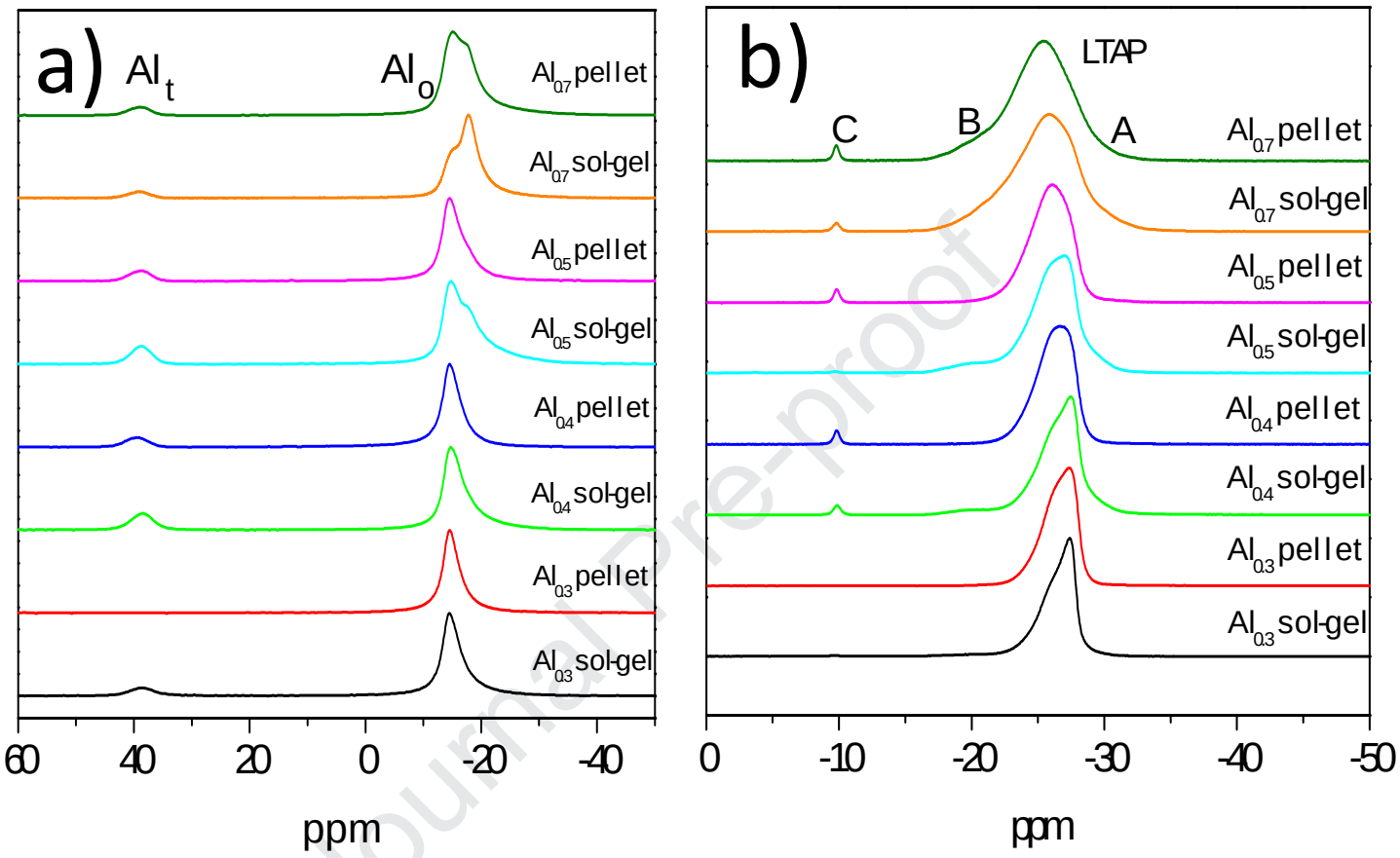


Figure 3

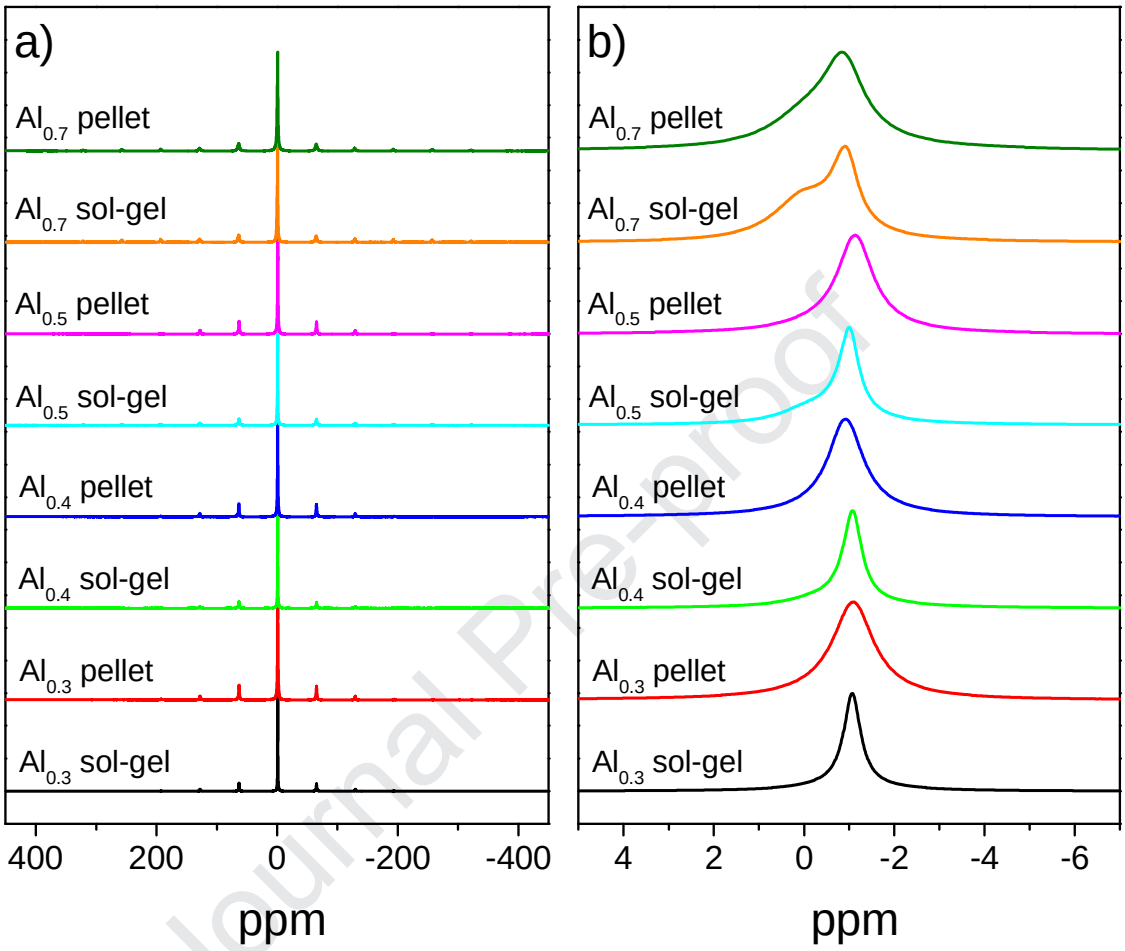


Figure 4

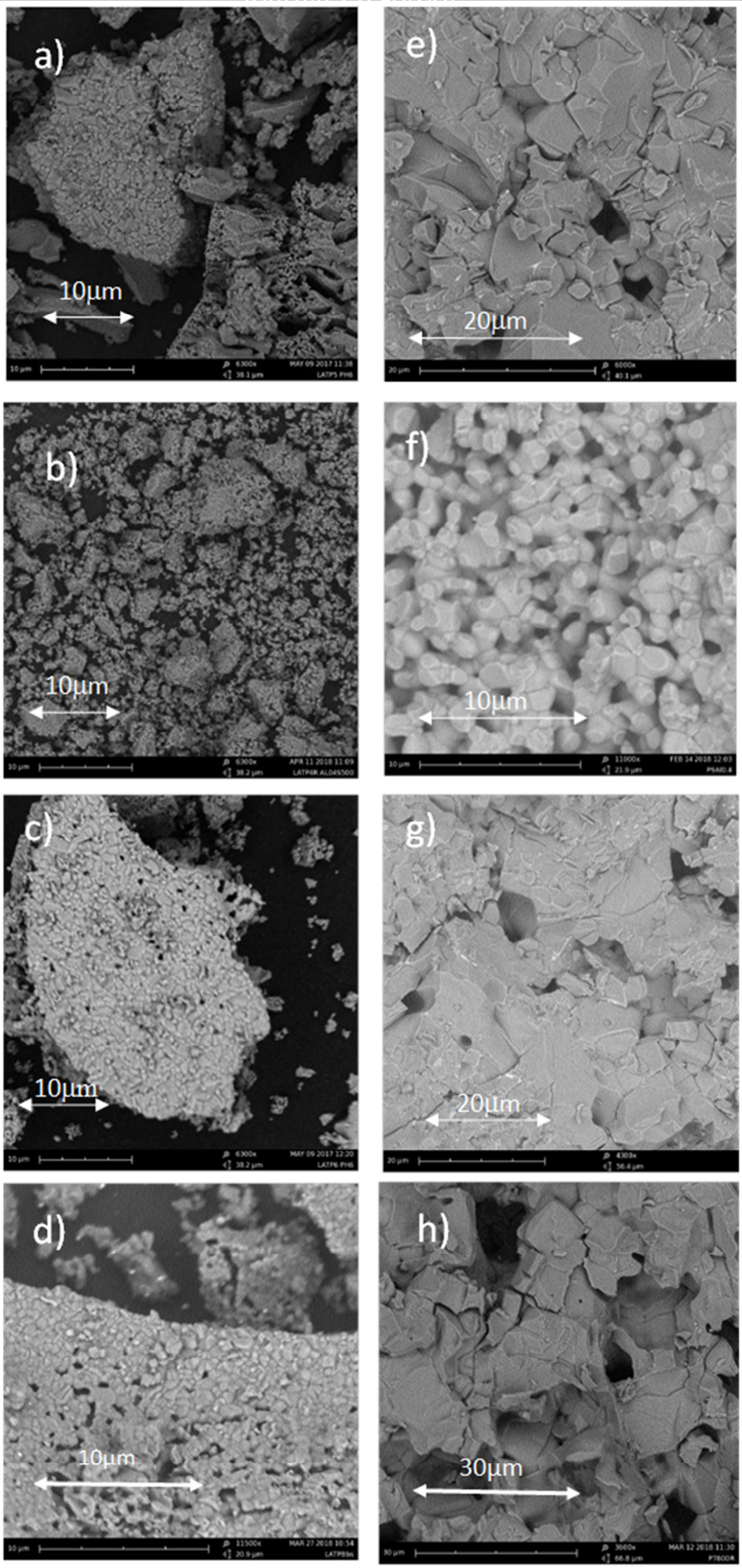


Figure 5

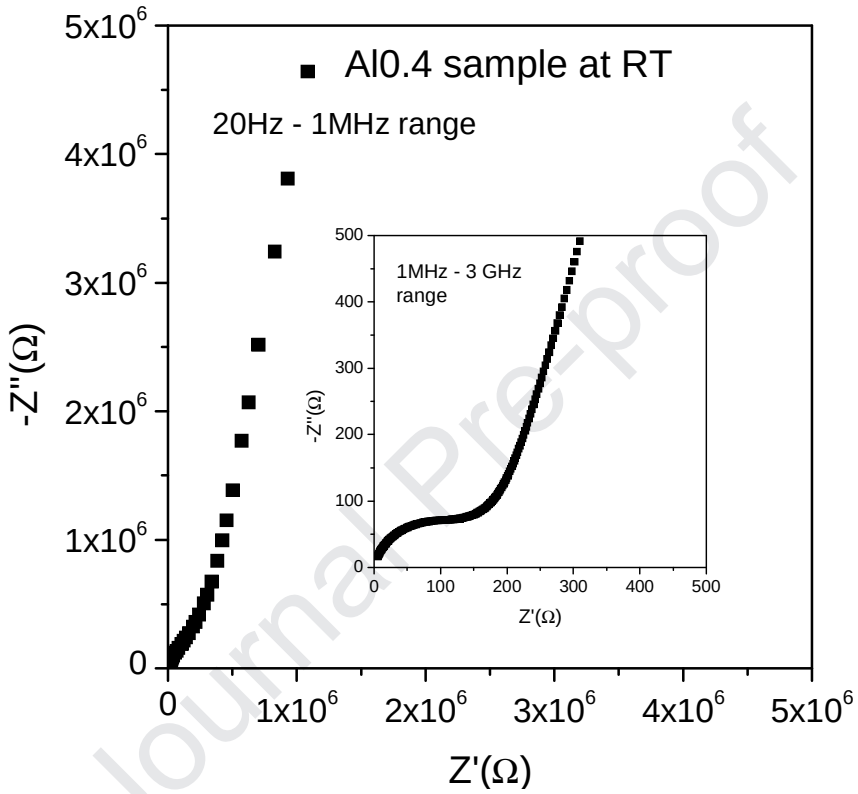


Figure 6

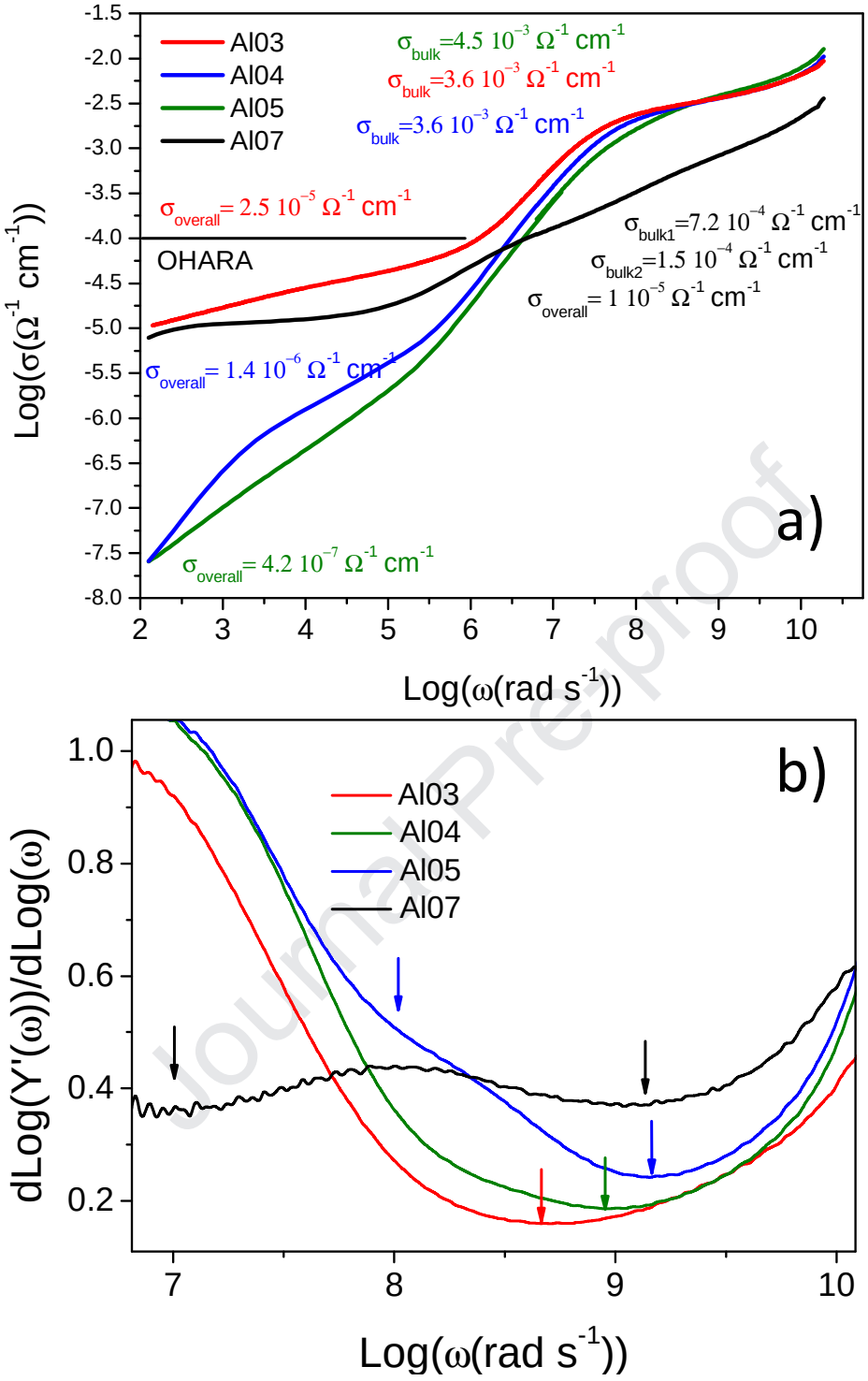


Figure 7

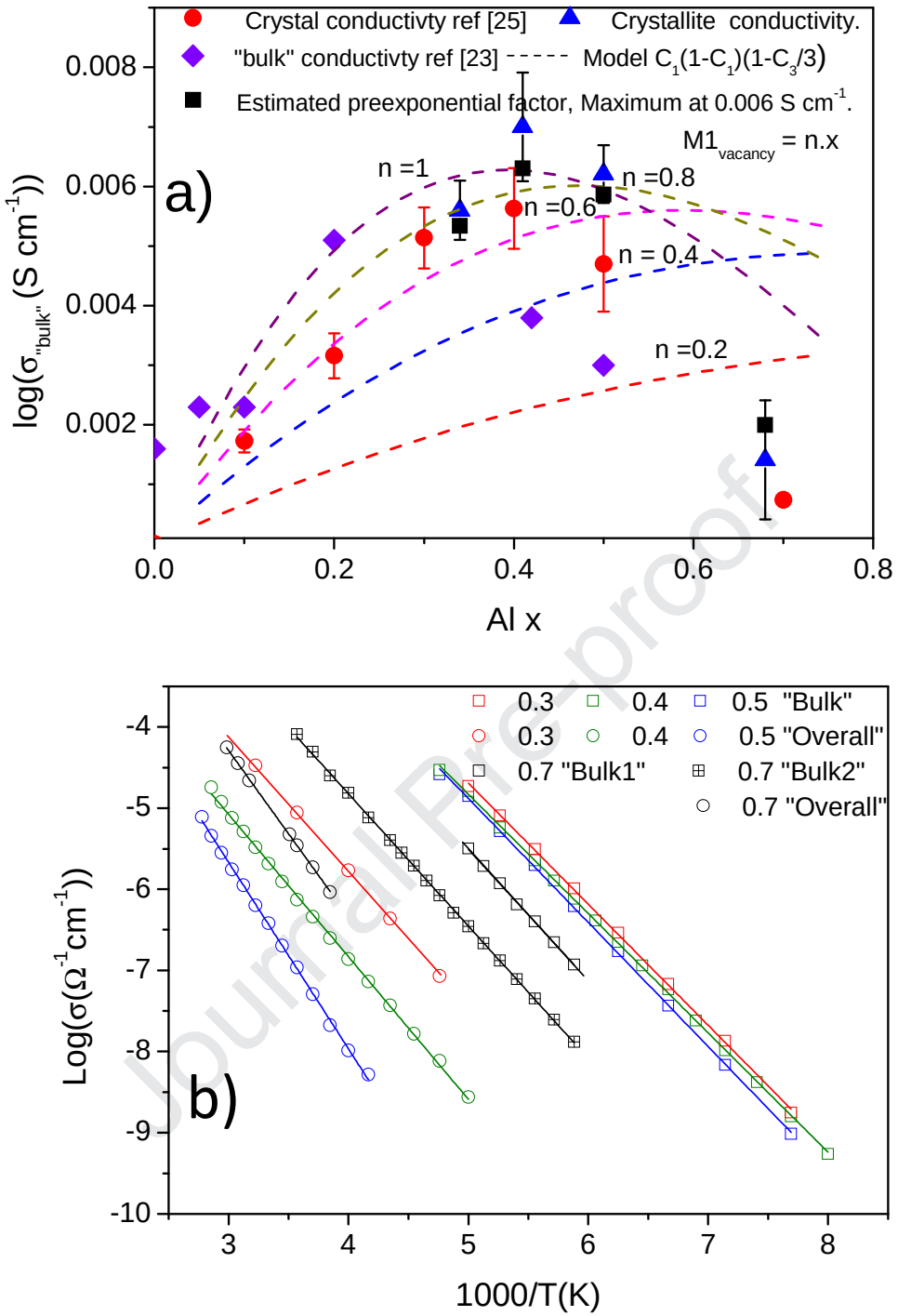


Figure 8

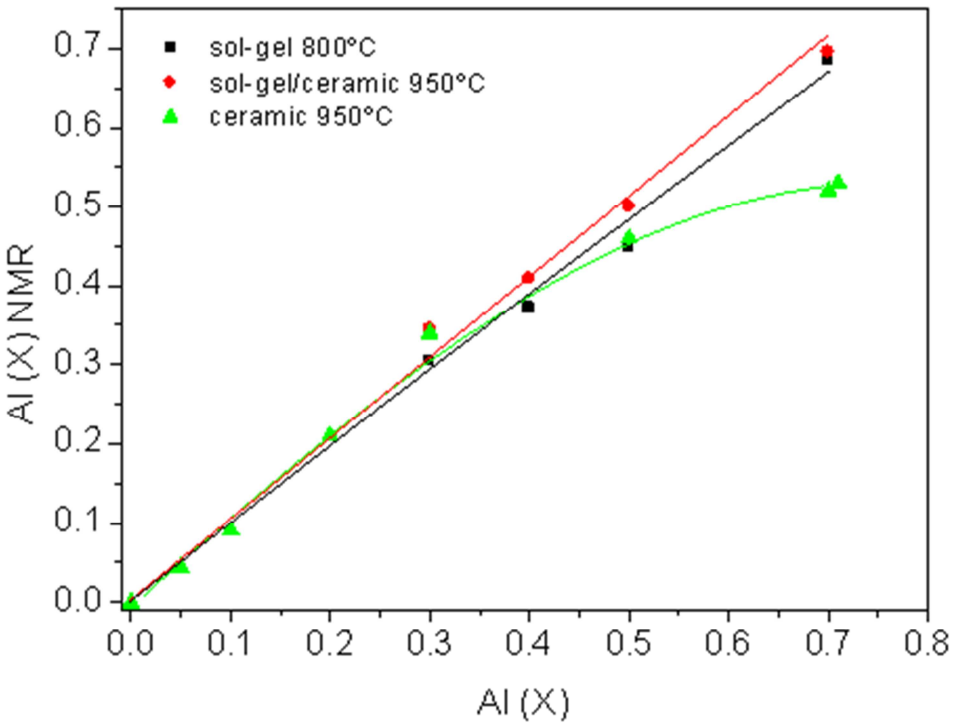


Figure 9

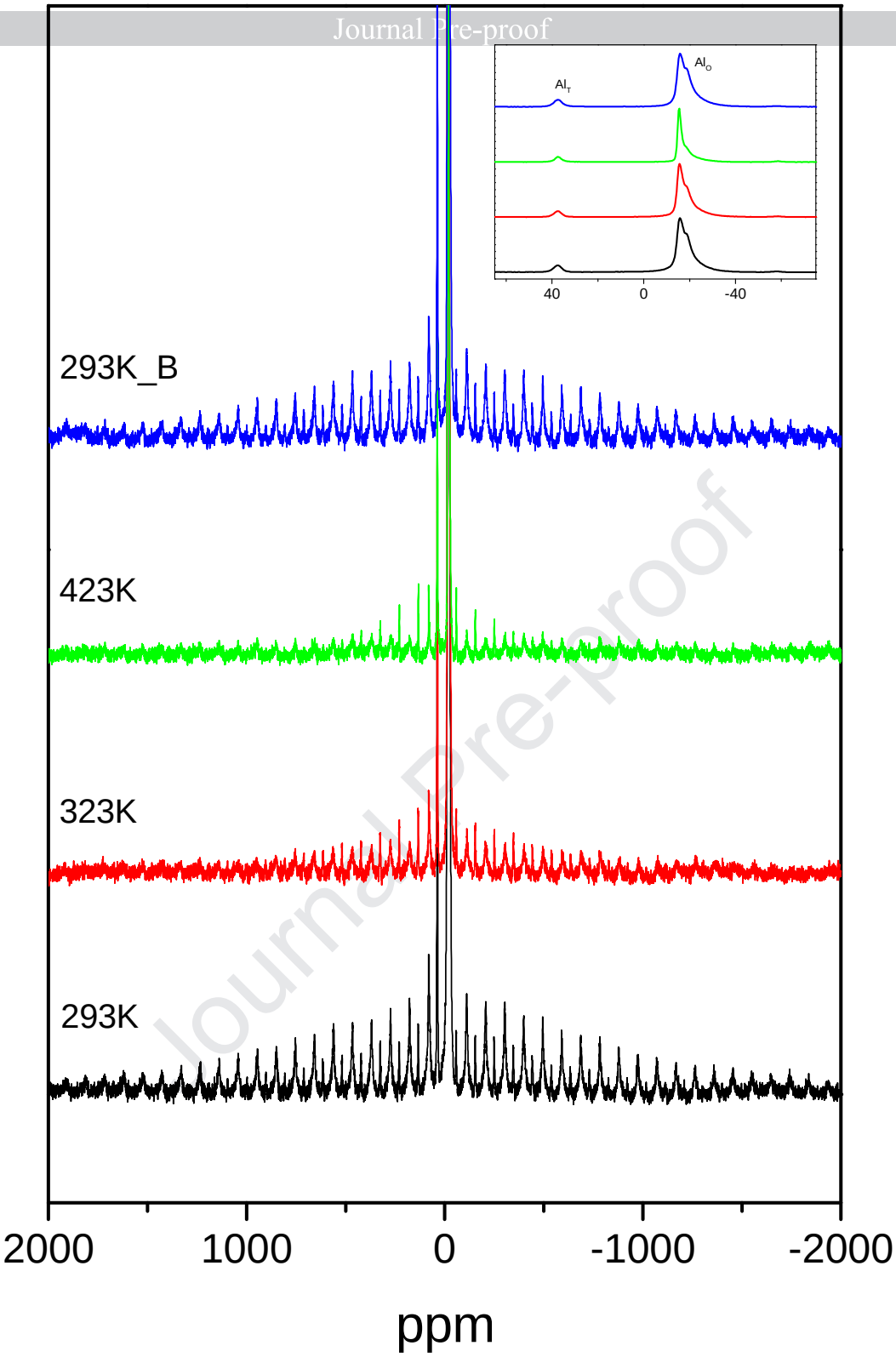


Figure 10

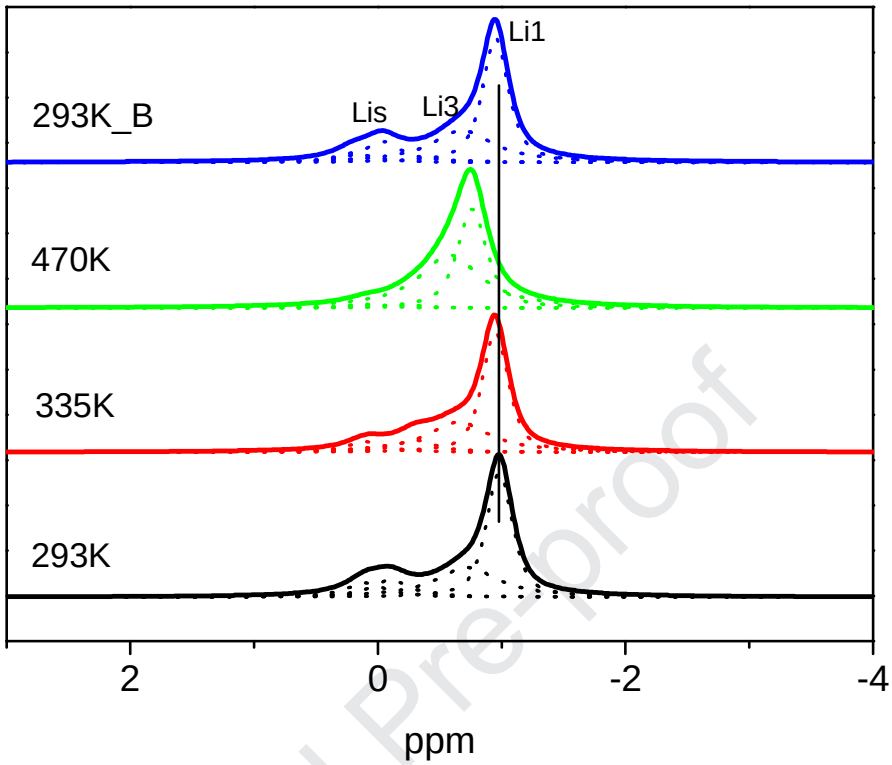


Figure 11

Highlights

1.- Sol-gel method enlarges the solid-solution limit in $Li_{1+x}Ti_{2-x}Al_x(PO_4)_3$

2.- Stoichiometry of compounds is close to nominal despite formation of secondary phases.

3.- Crystallite conductivity is maximum at x = 0.4, due to optimal Li distribution.

4.- A proposed jump probability model, reproduces the conductivity maximum at x = 0.4.

5.- The $^{27}Al$ NMR study indicates the non-random distribution of Ti / Al in the structure.

**Declaration of interests**

x The authors declare that they have no known competing financial interests or personal relationships that could have appeared to influence the work reported in this paper.

☐The authors declare the following financial interests/personal relationships which may be considered as potential competing interests: